

Testing the AGN unification model in the infrared. First results with GTC/CanariCam

Cristina Ramos Almeida^{1,2}

¹ Instituto de Astrofísica de Canarias, Calle Vía Láctea s/n, 38205, La Laguna, Tenerife

² Departamento de Astrofísica, Universidad de La Laguna, 38206, La Laguna, Tenerife

Abstract

The unified model for Active Galactic Nuclei (AGN) accounts for a variety of observational differences in terms of viewing geometry alone. However, from the fitting of high spatial resolution infrared (IR) data with clumpy torus models, it has been hinted that the immediate dusty surroundings of Type-1 and 2 Seyfert nuclei might be intrinsically different in terms of covering factor (torus width and number of clouds). Moreover, these torus covering factors also showed variations among objects belonging to the same type, in contradiction with simple unification. Interestingly, these intrinsic differences in Seyfert tori could explain, for example, the lack of broad optical lines in the polarized spectra of about half of the brightest Seyfert 2 galaxies. On the other hand, recent IR interferometry studies have revealed that, in at least four Seyfert galaxies, the mid-IR emission is elongated in the polar direction. These results are difficult to reconcile with unified models, which claim that the bulk of the mid-IR emission comes from the torus. In this invited contribution I summarize the latest results on high angular resolution IR studies of AGN, which constitute a crucial test for AGN unification. These results include those from the mid-infrared instrument CanariCam on the 10.4 m Gran Telescopio CANARIAS (GTC), which are starting to be published by the CanariCam AGN team, Los Piratas^a.

^a<https://sites.google.com/site/piratasrelatedpublications/>

1 Introduction

Observational evidence in the X-rays and the mid-infrared (MIR) indicates that the strong continuum source of active galactic nuclei (AGN) must be absorbed by obscuring material over a wide solid angle (see e.g., [4, 24, 42]). According to the observed spectra of different AGN types, the obscuring structure has to block the emission of the subparsec-scale broad-line region (BLR) where the broad lines are produced, but not that of the kiloparsec-scale

narrow-line region (NLR).

The unified model for active galaxies [5, 50] is based on the existence of a dusty toroidal structure surrounding the central region of an AGN. This toroidal geometry explains, for example, the biconical shapes observed in Hubble Space Telescope (HST) imaging of several AGNs [44, 25, 45] and also imaging and spectropolarimetric observations [4, 33]. Considering this geometry of the obscuring material, the central engines of Type-1 AGN can be seen directly, resulting in typical spectra with both narrow and broad emission lines, whereas in Type-2 AGN the BLR is obscured.

According to MIR interferometry, the dusty torus of Seyfert galaxies is only a few parsecs across ($R_{\text{outer}} < 10$ pc; see [8] and references therein). Because of its small size, even with 10 m-class telescopes we do not have a direct image of the torus, and we have to rely on models to reproduce the spectral energy distribution (SED) of Seyfert galaxies to derive the torus properties.

The infrared (IR) range (and particularly the MIR) is key to set constraints on torus models, since the reprocessed radiation from the dust in the torus is re-emitted in this range. However, when comparing the predictions of any torus model with observations, the torus small-scale emission must be isolated. High angular resolution is then essential to separate torus emission from stellar emission and star-heated dust in the near-IR (NIR) and MIR, respectively. Such observations are also crucial for disentangling the relation between nuclear activity and star formation on scales of tens of parsecs [12].

Seyfert galaxies are ideal laboratories for 1) constraining torus properties by fitting their nuclear SEDs with models and 2) studying the interplay between nuclear activity and star formation on nuclear scales thanks to the Polycyclic Aromatic Hydrocarbon (PAH) features that dominate the MIR spectra of star-forming galaxies. In this contribution I will first review three observational results that challenge the AGN unification model, and second, I will summarize the first results based on MIR data from the instrument CanariCam on the 10.4 m Gran Telescopio CANARIAS (GTC), which are helping us to better understand the connection between nuclear activity and star formation in the local universe.

2 Challenges to simple unification

Although widely accepted by the community and successful in explaining several AGN observational properties, the unification model is not unchallenged, and in fact, in the last years, a number of publications seem to argue against simple unification. In this section I will summarize three of them.

2.1 Differences in torus covering factor

In [37, 38] we fitted the nuclear IR SEDs of 20 nearby Seyfert galaxies using the clumpy torus models of [31, 32] and a Bayesian approach [6, 7] to derive their torus parameters. The combination of larger number of clumps and broader tori implies more efficient reprocessors and higher covering factors than those with lower values of these parameters. Despite the

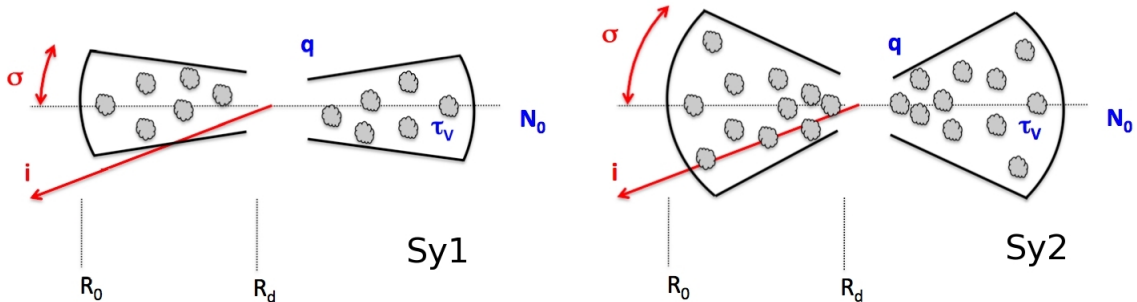


Figure 1: Different clumpy tori for different AGN types. The Type-1 torus (*left* panel) is narrower and it has lower number of clumps than the Type-2 torus (*right* panel). Figure adapted from [39].

limited number of galaxies considered, we found that Type-2 tori have larger covering factors, and therefore are more efficient reprocessors, than those of Type-1. In addition, we find intermediate values of the orientation of the torus with respect to our line-of-sight, and not face-on and edge-on tori for Seyfert 1 and 2 galaxies, respectively, as simple unification predicts. If these findings are confirmed for a statistically significant sample of Seyfert galaxies, they immediately imply that is not only torus orientation what determines the classification of an AGN as Type-1 or Type-2, but also the intrinsic properties the torus. It is more likely to have an AGN classified as a Type-1 if the torus has fewer clumps and it is narrower and viceversa (see Fig. 1).

2.2 Dust in the polar direction

Torus models predict that the torus emission peaks in the MIR ($\sim 20 - 30 \mu\text{m}$; e.g. [31, 32]). However, recent MIR interferometric observations at subarcsecond resolution revealed that the bulk of the MIR emission in four Seyfert galaxies is elongated in the polar direction [35, 18, 19, 49]. This small sample includes one Seyfert 1 (NGC 3783) and three Seyfert 2 galaxies (Circinus, NGC 424 and NGC 1068). According to the observations, 60 – 90% of the nuclear MIR emission ($< 10 \text{ pc}$) arises from the polar region, with a strong dependence on wavelength. The longer the wavelength, the more important the polar component and the less important the disk component that would be associated with the torus (see left panel of Fig. 2; [19]). According to [19], the two peaks at $\sim 3 - 5$ and $\sim 20 \mu\text{m}$ observed in the IR SED of some Seyfert galaxies (see right panel of Fig. 2) would be produced by the small, hot inner disk and the larger polar components, respectively.

It is noteworthy that this parsec-scale MIR polar emission connects to the extended polar dust emission found in a large number of AGN on scales of $\sim 10 - 100 \text{ pc}$, also using MIR observations (e.g. [34, 17]).

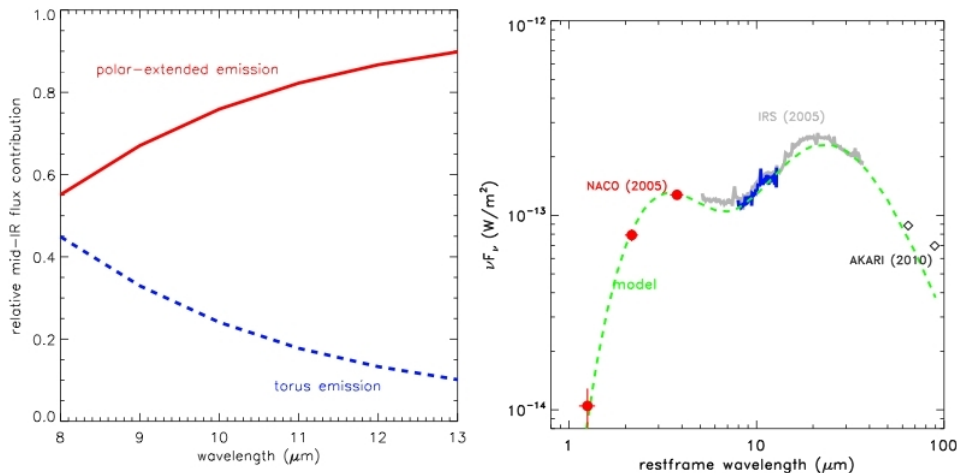


Figure 2: *Left panel:* Contributions from the polar extended component (red solid line) and compact torus emission (blue dashed line). The longer the wavelength, the more important the polar component. *Right panel:* IR SED of the Seyfert 1 galaxy NGC 3783, showing two peaks at $\sim 3 - 5$ and $\sim 20 \mu\text{m}$, which would correspond to the polar and torus components respectively. Figures from [19].

2.3 Hidden and non-hidden BLR

The AGN unification model first proposed by [5] stems from the detection of polarized broad lines in the nucleus of the Seyfert 2 galaxy NGC 1068 [4]. The radiation escapes through conical beams aligned perpendicularly to the torus, and part of it is scattered towards us, producing the linearly polarized broad lines observed in the spectrum of NGC 1068. After this discovery, a search for the polarized broad lines of nearby Seyfert 2 galaxies started, but to date, only $\sim 40\%$ of the targets that have been observed show a Seyfert 1 polarized spectrum in the optical [47, 48, 28]. This might imply that either not all Seyfert 2s harbor a BLR [47, 48, 15] or the nuclear dust distribution is not as simple as the unification model predicts (e.g. [27, 16]). In a recent work, [21] reported differences between the torus covering factors of Seyfert 2 galaxies with and without polarized broad lines.

An alternative to the two scenarios described above is the quality of previous spectropolarimetry. There are few spectropolarimetric observations of Seyfert galaxies reported in the literature, and the overall majority of those observations have relatively low signal-to-noise (S/N) ratios, because they were obtained with small telescopes (3 – 4 m; e.g. [51, 23]). Thus, in order to characterize and properly compare the linear polarization properties of individual Seyfert 2 galaxies, a homogeneous data set of observations obtained with the same sensitivity and S/N is required. A $S/N \sim 300$ in line intensity is the minimum necessary to detect the linear polarization signal (1 – 5%) typical of Seyfert galaxies [4] at the 3σ level. With this aim, we have obtained a homogeneous dataset of linearly polarized optical spectra for a representative flux-limited subsample of 15 Seyfert 2 galaxies for which we have their torus properties constrained thanks to our previous work [37, 38, 1]. The spectropolarimetric observations were taken with the instrument FORS2 on the 8 m Very Large Telescope (VLT) in 2013 April. The sample includes targets previously classified as hidden BLR (HBLR), non-

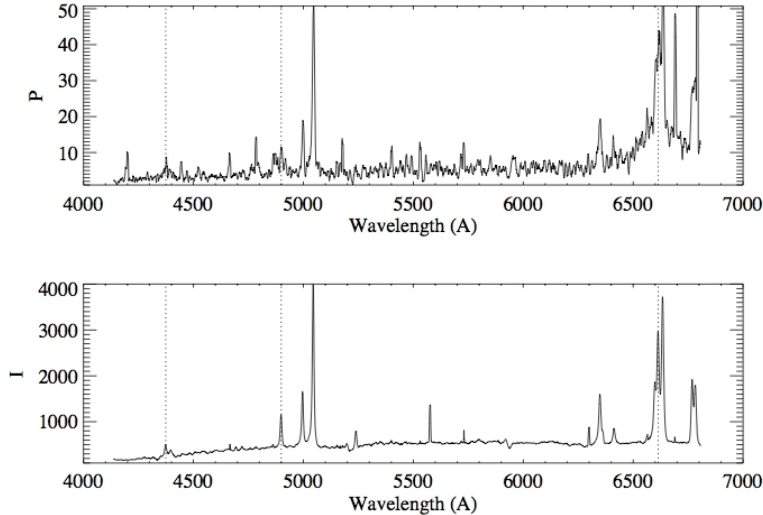


Figure 3: *Top* and *bottom* panels correspond to the linearly polarized and total flux spectra of the Seyfert 2 galaxy NGC 2110, respectively. Dotted vertical lines correspond to the central position of $H\alpha$, $H\beta$ and $H\gamma$. These three recombination lines clearly show broad pedestals in the polarized flux spectrum, indicating the presence of a hidden BLR. Figure from [41].

hidden BLR (NHBLR) and others without published spectropolarimetry data but classified as NHBLR.

From the analysis of our VLT/FORS2 spectropolarimetric observations, we find that all the galaxies show broad components of the recombination lines ($H\alpha$ and $H\beta$ in 13 of the galaxies and only $H\alpha$ in the other two). Twelve of the galaxies show polarized broad lines with full-widths at half maximum (FWHM) $> 2000 \text{ km s}^{-1}$, typical of Seyfert 1 galaxies (see Fig. 3), whereas the other three have broad components of FWHM $< 2000 \text{ km s}^{-1}$, still broader than the typical NLR lines ($\sim 500 \text{ km s}^{-1}$), but more similar to the intermediate components of $\sim 1500 \text{ km s}^{-1}$ detected in the NIR spectrum of some Seyfert 2 galaxies (e.g. [30, 36]). These intermediate-width lines are thought to come from a transition region between the NLR and the BLR. Alternatively, these galaxies could be the obscured counterparts of narrow-line Seyfert 1 galaxies (NLSy1), whose broad components have typical FWHM $< 2000 \text{ km s}^{-1}$, as measured from their total flux spectra. These results are still preliminary, and they will be published in [41].

3 First results with GTC/CanariCam

During the last decade, the number of AGN studies has increased significantly as a consequence of the impact that they seem to have on their host galaxies. For example, there is theoretical and observational evidence for AGN quenching star formation through the so-

called AGN feedback (see e.g. [14, 43]), although this quenching is not ubiquitous and the physical scales on which it takes place are not clear yet. Indeed, it is known that star formation takes place on kpc-scales and down to tens of parsecs from the nuclei of Seyfert galaxies [10, 9, 22, 3, 12].

Numerical simulations predict a relation with some scatter between the star formation rates (SFRs) on different galaxy scales (between 10 kpc and 1 pc) and black hole accretion rates [20]. However, the lack of angular resolution of previous observations prevented a clear comparison on scales of tens of parsecs. Ground-based MIR observations with 8 – 10 m-class telescopes might then hold the key for disentangling the relation between nuclear activity and star formation in the nuclear region of Seyfert galaxies. With this aim, we are conducting a MIR imaging and spectroscopic survey of ~ 100 local AGN using the instrument CanariCam (CC; [46]) on the 10.4 m GTC, in La Palma. The data were taken as part of the 100 hours of guaranteed time observations (coordinator: Packham) and an ESO/GTC large programme (182.B-2005; P.I: Alonso-Herrero) awarded 180 hours of GTC/CC time. The sample includes both high-to-intermediate luminosity AGN (PG quasars, radio galaxies and Seyfert galaxies) and low-luminosity AGN (low-ionization nuclear emission-line regions; LINERs) covering almost six orders of magnitude in AGN luminosity (see [2] for further details). Publications to date based on the GTC/CC guaranteed time and ESO/GTC observations include [2, 3, 29, 40, 13, 26]. In the following sections, I will summarize the results presented in [3, 40, 13].

3.1 AGN dilution of the 11.3 μm PAH feature.

Among the galaxies in our survey already observed with GTC/CC, we first selected five Seyfert galaxies for which there was evidence in the literature of nuclear star formation and that show extended MIR emission in the CC 8.7 μm images (see Fig. 4). We obtained MIR spectroscopy in the range 7.5 – 13 μm for all of them and found extended PAH emission [3, 40]. The equivalent width (EW) of the 11.3 μm PAH feature shows a minimum at the galaxy nuclei but increases with radial distance, reaching typical star-forming values a few hundred parsecs away from the AGN nucleus (see left panel of Fig. 5). The small nuclear EWs are interpreted as due to increased dilution from the AGN continuum rather than destruction of the PAH molecules, as previously suggested in the literature. We conclude that at least the carriers of the 11.3 μm PAH survive in nuclear environments as close as 10 pc from the AGN in Seyfert galaxies [3, 12, 40].

In [40] we studied in detail the extended MIR emission of the galaxy Mrk 1066, which is also included in the sample analysed in [3]. For this galaxy, we subtracted the AGN unresolved component from the 8 – 13 μm GTC/CC spectra of the star-forming knots and the nucleus, and measured EWs of the 11.3 μm PAH feature which are typical of pure starburst galaxies. Indeed, this EW is larger in the nucleus than in the knots (see right panel of Fig. 5), confirming that the AGN dilutes the PAH emission, but does not destroy the carriers of 11.3 μm PAH.

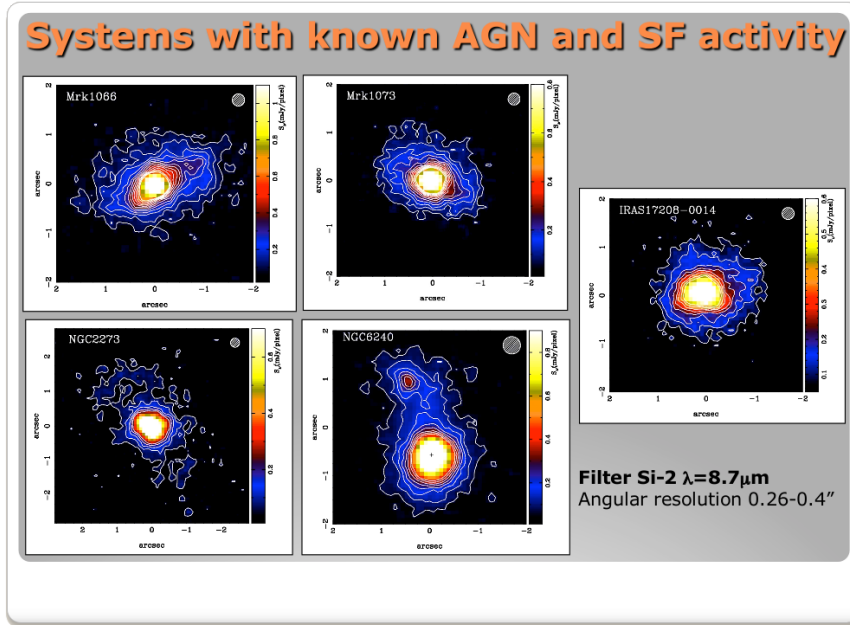


Figure 4: GTC/CC Si-2 ($\lambda_c = 8.7 \mu\text{m}$) images of the five Seyfert galaxies studied in [3]. Orientation is north up, east to the left. The contours are in a linear scale with the lowest contour corresponding to the local background value plus 1.5 standard deviations measured in the image before rotating the images. Hatched circles represent the angular resolution of the image (FWHM) approximated as a Gaussian function. Figure adapted from [3].

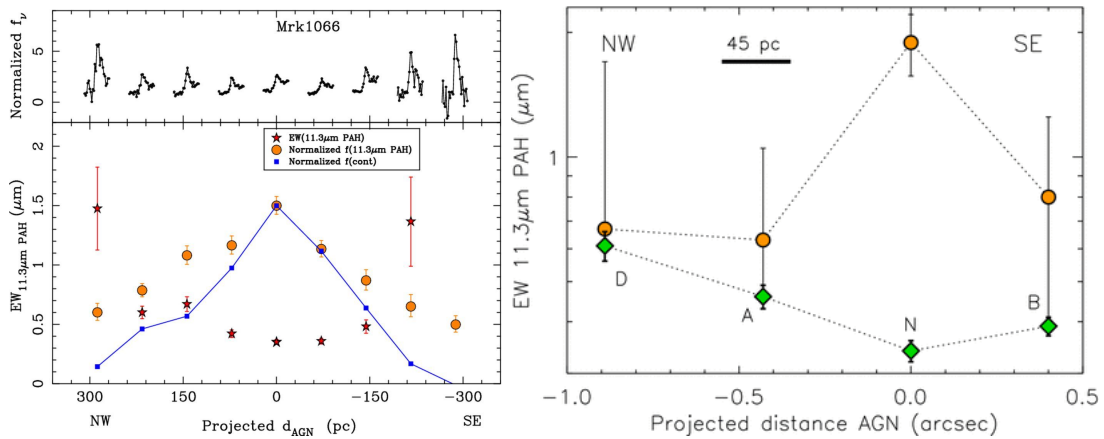


Figure 5: *Left panel*: Spatial profiles of Mrk1066, obtained from GTC/CC spectra, as a function of the projected distance from the AGN. Stars and filled dots correspond to EW and flux of the $11.3 \mu\text{m}$ PAH feature respectively, and filled squares to the flux of the local continuum at $11.25 \mu\text{m}$. Top panel shows the normalized spectra around the $11.3 \mu\text{m}$ PAH feature at different projected distances. Figure from [3]. *Right panel*: Spatial variation of the $11.3 \mu\text{m}$ PAH feature EW before and after subtracting the AGN component (green diamonds and orange circles, respectively). Figure from [40].

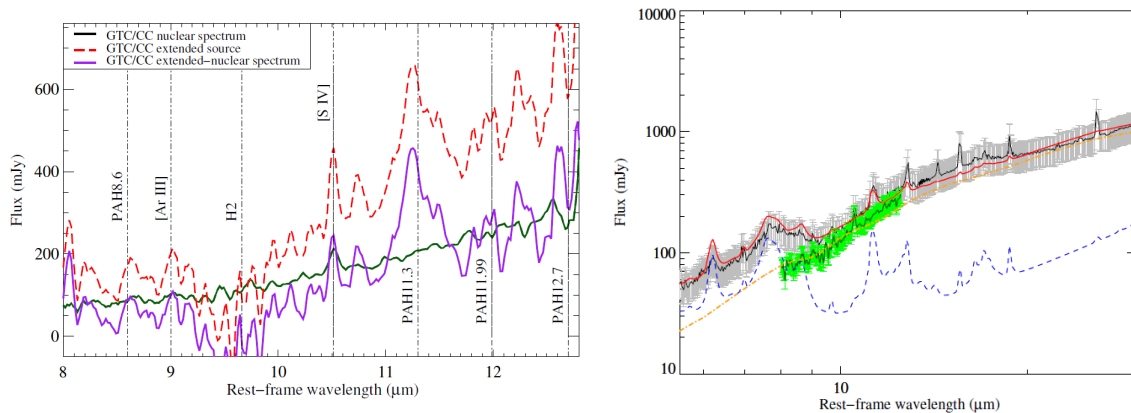


Figure 6: *Left panel:* GTC/CC spectrum of NGC 2992 extracted in an aperture radius of $5.2'' \sim 900$ pc (red dashed line), GTC/CC nuclear spectrum (green solid line) and spectrum of the extended emission (purple solid line), obtained by subtracting the nuclear from the extended emission spectrum. *Right panel:* Spitzer/IRS spectrum of NGC 2992 (black solid line), best fit (red solid line) and AGN and starburst templates (orange dot-dashed and blue dashed lines respectively). The GTC/CC nuclear spectrum is shown for comparison (green thick line). Figures from [13].

3.2 The nuclear and extended IR emission of the Seyfert galaxy NGC 2992.

Another target that has been observed with GTC/CC as part of our ESO/GTC large programme is the Seyfert 1.9 galaxy NGC 2992. This nearby AGN is part of the interacting system Arp 245, together with the star-forming spiral galaxy NGC 2993 and the tidal dwarf galaxy Arp 245 North. Two bright tidal features connect these three galaxies, suggesting that the system is in an early stage of the interaction [11].

In [13] we presented subarcsecond resolution MIR imaging and spectroscopic observations of NGC 2992, obtained with GTC/CC and with Michelle on the 8 m Gemini North telescope. The imaging data revealed extended emission along the major axis of the galaxy out to ~ 3 kpc. By comparing the GTC/CC nuclear MIR spectrum of the galaxy with that of the extended emission, we concluded that the origin of the latter is dust in the inner galaxy disk, with some contribution from star formation (see left panel of Fig. 6).

We also studied MIR and far-IR (FIR) imaging data of the interacting system Arp 245 obtained with the Spitzer Space Telescope and the Herschel Space Observatory. We obtained nuclear MIR and FIR fluxes and compared them with the subarcsecond resolution MIR data, and concluded that we can only recover the nuclear fluxes at $20 - 25 \mu\text{m}$, where the AGN emission dominates. We also decomposed the Spitzer spectrum of NGC 2992, which probes the inner ~ 600 pc of the galaxy, in AGN and starburst components. Using this method, we find that the scaled AGN template coincides in flux and spectral shape with the GTC/CC nuclear spectrum. This proves the reliability of this technique to estimate the AGN and starburst fractional contributions in the wavelength range covered by Spitzer ($5 - 35 \mu\text{m}$; see right panel of Fig. 6).

Acknowledgments

CRA is supported by a Marie Curie Intra European Fellowship within the 7th European Community Framework Programme (PIEF-GA-2012-327934). CRA also acknowledges financial support from the Instituto de Astrofísica de Canarias and the Spanish Ministry of Science and Innovation (MICINN) through project PN AYA2010-21887-C04.04 (Estallidos). The author finally acknowledges Almudena Alonso-Herrero and Sebastian Hönig for useful comments.

References

- [1] Alonso-Herrero, A., Ramos Almeida, C., Mason, R., et al. 2011, *ApJ*, 736, 82
- [2] Alonso-Herrero, A., Roche, P. F., Esquej, P., et al. 2013, *ApJ*, 779, L14
- [3] Alonso-Herrero, A., Ramos Almeida, C., Esquej, P., et al. 2014, *MNRAS*, 443, 2766
- [4] Antonucci, R. R. J., & Miller, J. 1985, *ApJ*, 297, 621
- [5] Antonucci, R. R. J. 1993, *ARA&A*, 31, 473
- [6] Asensio Ramos, A., & Ramos Almeida, C. 2009, *ApJ*, 696, 2075
- [7] Asensio Ramos, A., & Ramos Almeida, C. 2013, *MNRAS*, 428, 195
- [8] Burtscher, L., Meisenheimer, K., Tristram, K. R. W., et al. 2013, *A&A*, 558, 149
- [9] Diamond-Stanic, A. M., & Rieke, G. H. 2012, *ApJ*, 746, 168
- [10] Diamond-Stanic, A. M., & Rieke, G. H. 2010, *ApJ*, 724, 140
- [11] Duc, P.-A., Brinks, E., Springel, V., et al. 2000, *AJ*, 120, 1238
- [12] Esquej, P., Alonso-Herrero, A., González-Martín, O., et al. 2014, *ApJ*, 780, 86
- [13] García-Bernete, I., Ramos Almeida, C., Acosta-Pulido, J. A., et al. 2015, *MNRAS*, submitted
- [14] Granato, G. L., De Zotti, G., Silva, L., Bressan, A., & Danese, L. 2004, *ApJ*, 600, 580
- [15] Gu, Q., & Huang, J. 2002, *ApJ*, 579, 205
- [16] Heisler, C. A., Lumsden, S. L., & Bailey, J. A. 1997, *Nature*, 385, 700
- [17] Hönig, S. F., Kishimoto, M., Gandhi, P., et al. 2010, *A&A*, 515, 23
- [18] Hönig, S. F., Kishimoto, M., Antonucci, R., et al. 2012, *ApJ*, 755, 149
- [19] Hönig, S. F., Kishimoto, M., Tristram, K. R. W., et al. 2013, *ApJ*, 771, 87
- [20] Hopkins, P. F., & Quataert, E. 2010, *MNRAS*, 407, 1529
- [21] Ichikawa, K., Packham, C., Ramos Almeida, C., et al. 2015, *ApJ*, submitted
- [22] LaMassa, S. M., Heckman, T. M., Ptak, A., et al. 2012, *ApJ*, 758, 1
- [23] Lumsden, S. L., Alexander, D. M., & Hough, J. H. 2004, *MNRAS*, 348, 1451
- [24] Maiolino, R., Salvati, M., Bassani, L., et al. 1998, *A&A*, 338, 781
- [25] Malkan, M. A., Gorjian, V., & Tam, R. 1998, *ApJS*, 117, 25
- [26] Martinez Paredes, M., Alonso-Herrero, A., Aretxaga, I., et al. 2015, *MNRAS*, in prep.

- [27] Miller, J. S. & Goodrich, R. W. 1990, *ApJ*, 355, 456
- [28] Moran, E. C., Kay, L. E., Davis, M., Filippenko, A. V., & Barth, A. J., 2001, *ApJ*, 556, L75
- [29] Mori, T. I., Imanishi, M., Alonso-Herrero, A., et al. 2014, *PASP*, 66, 93
- [30] Nagar, N. M., Oliva, E., Marconi, A., & Maiolino, R. 2002, *A&A*, 391, L21
- [31] Nenkova, M., Sirocky, M. M., Ivezić, Ž., & Elitzur, M. 2008a, *ApJ*, 685, 147
- [32] Nenkova, M., Sirocky, M. M., Nikutta, R., Ivezić, Ž., & Elitzur, M. 2008b, *ApJ*, 685, 160
- [33] Packham, C., Young, S., Hough, J. H., Axon, D. J., & Bailey, J. A. 1997, *MNRAS*, 288, 375
- [34] Packham, C., Radomski, J. T., Roche, P. F., et al. 2005, *ApJ*, 618, L17
- [35] Raban, D., Jaffe, W., Röttgering, H., Meisenheimer, K., & Tristram, K. R. W. 2009, *MNRAS*, 394, 1325
- [36] Ramos Almeida, C., Pérez García, A. M., Acosta-Pulido, J. A., & González-Martín, O. 2008, *ApJ*, 680, L17
- [37] Ramos Almeida, C., Levenson, N. A., Rodríguez Espinosa, J. M., et al. 2009, *ApJ*, 702, 1127
- [38] Ramos Almeida, C., Levenson, N. A., Alonso-Herrero, A., et al. 2011, *ApJ*, 731, 92
- [39] Ramos Almeida, C., Alonso-Herrero, A., Levenson, N. A., et al. 2014b, *MNRAS*, 439, 3847
- [40] Ramos Almeida, C., Alonso-Herrero, A., Esquej, P., et al. 2014a, *MNRAS*, 445, 1130
- [41] Ramos Almeida, C., Martínez-González, M. J., Asensio Ramos, A., et al. in preparation
- [42] Risaliti, G., Elvis, M., & Nicastro, F. 2002, *ApJ*, 571, 234
- [43] Springel, V., Di Matteo, T., & Hernquist, L. 2005, *MNRAS*, 361, 776
- [44] Tadhunter, C., & Tsvetanov, Z. 1989, *Nature*, 341, 422
- [45] Tadhunter, C. N., Packham, C., Axon, D. J., et al. 1999, *ApJ*, 512, L91
- [46] Telesco, C. M., Ciardi, D., French, J., et al. 2003, *Proc. SPIE*, 4841, 913
- [47] Tran, H. D. 2001, *ApJ*, 554, L19
- [48] Tran, H. D. 2003, *ApJ*, 583, 632
- [49] Tristram, K. R. W., Burtscher, L., Jaffe, W., et al. 2014, *A&A*, 563, 82
- [50] Urry, C. M., & Padovani, P. 1995, *PASP*, 107, 803
- [51] Watanabe, M., Nagata, T., Sato, S., Nakaya, H., & Hough, J. H. 2003, *ApJ*, 591, 714